AGU ADVANCING EARTH AND SPACE SCIENCE

Geophysical Research Letters

RESEARCH LETTER
10.1029/2020GL090255

Deformation Precursors to Catastrophic Failure in Rocks

J. A. McBeck[1], J. M. Aiken[2,3], J. Mathiesen[4], Y. Ben-Zion[5], and F. Renard[1,6]

[1]Physics of Geological Processes, Department of Geosciences, The Njord Centre, University of Oslo, Oslo, Norway, [2]Department of Physics, Center for Computing in Science Education, University of Oslo, Oslo, Norway, [3]Department of Physics and Astronomy, Michigan State University, East Lansing, MI, USA, [4]Niels Bohr Institute, University of Copenhagen, Copenhagen, Denmark, [5]Department of Earth Sciences, University of Southern California, Los Angeles, CA, USA, [6]University Grenoble Alpes, University Savoie Mont Blanc, CNRS, IRD, IFSTTAR, ISTerre, Grenoble, France

Abstract Forecasting the timing of catastrophic failure, such as crustal earthquakes, has been a central concern for centuries. Such forecasting requires identifying signals that evolve or accelerate in the precursory phase leading to failure, and the subset of signals that may be detected in the crust. We develop machine learning models to predict the proximity of catastrophic failure in synchrotron X-ray tomography triaxial compression experiments on rocks using characteristics of evolving fracture networks. We then examine the characteristics that most strongly influence the model results, and thus may be considered the best predictors of the proximity of macroscopic failure. The resulting suite of predictive parameters underscores the importance of dilation in the precursory phase leading to catastrophic failure. The results indicate that the evolution of the strain energy density field may provide more robust predictions of the proximity of failure than other existing metrics of rock deformation.

Plain Language Summary What controls the timing of large earthquakes? Estimating the conditions conducive to the next large earthquake can help mitigate seismic hazard and save significant societal and economic costs. A prerequisite for such estimates includes determining what measurable and detectable signals change in a systematic manner in rocks approaching catastrophic failure. Machine learning analyses of data acquired by synchrotron X-ray experiments on rocks provide robust means of identifying the evolving fault network characteristics that best predict the proximity of catastrophic failure of the rocks. Translating these fracture network characteristics to geophysical signals may help scientists detect such precursors within crustal fault systems preceding large earthquakes.

Key Points:

- X-ray tomography during triaxial compression reveal evolving fracture network characteristics leading to catastrophic failure in rocks
- Machine learning methods identify fracture characteristics that best signal the proximity of catastrophic failure
- The strain energy density field (off-fault deformation) may provide the most accurate predictions of failure proximity of existing criteria

Supporting Information:

- Supporting Information S1

Correspondence to:
J. McBeck,
j.a.mcbeck@geo.uio.no

Citation:
McBeck, J. A., Aiken, J. M., Mathiesen, J., Ben-Zion, Y., & Renard, F. (2020). Deformation precursors to catastrophic failure in rocks. *Geophysical Research Letters*, *47*, e2020GL090255. https://doi.org/10.1029/2020GL090255

Received 13 AUG 2020
Accepted 26 NOV 2020

1. Introduction

Predicting the proximity of future destructive earthquakes is a fundamental goal of science, with significant challenges and societal importance. A key aspect of this prediction is identifying the signals that may be detectable in situ before catastrophic failure. The dilatancy-diffusion hypothesis predicts that as fractures open and propagate in the crust in the presence of fluids, larger ratios of fluid to solid volume develop (Nur, 1974). This increased ratio is expected to reduce the *P* wave and *S* wave seismic velocities and effective elastic moduli, and alter local hydrologic levels. Such variations in geophysical signals have been observed prior to some earthquakes (Aggarwal et al., 1973; Frank, 1965; Roeloffs, 1988; Whitcomb et al., 1973). However, this idea has remained a controversial hypothesis, likely because some earthquakes do not appear to have such precursors (Amoruso & Crescentini, 2010; Bolt, 1977; Cicerone et al., 2009; Haase et al., 1995; McEvilly & Johnson, 1974).

In recent years, analyses have used machine learning to predict the timing of earthquakes and their laboratory analogs (e.g., Rouet-Leduc et al., 2017; Corbi et al., 2019; Hulbert et al., 2019). However, to our knowledge, none have used characteristics of evolving fracture networks to perform such predictions, and thus none have identified which of these characteristics may be potential geophysical precursors. Here, we aim to identify the deformation phenomena that may signal the proximity of catastrophic failure in rocks. We develop machine learning models to predict the proximity to failure in eight triaxial compression experiments on rocks representative of the crystalline continental crust: marble, monzonite, and granite (Table S1). In situ synchrotron X-ray tomography triaxial compression experiments (e.g., Renard et al., 2016) provide images of 3-D fracture networks at 26–88 differential stress steps approaching dynamic failure in these eight experiments (Figures 1, S1, and Table S2). To characterize these evolving fracture networks,

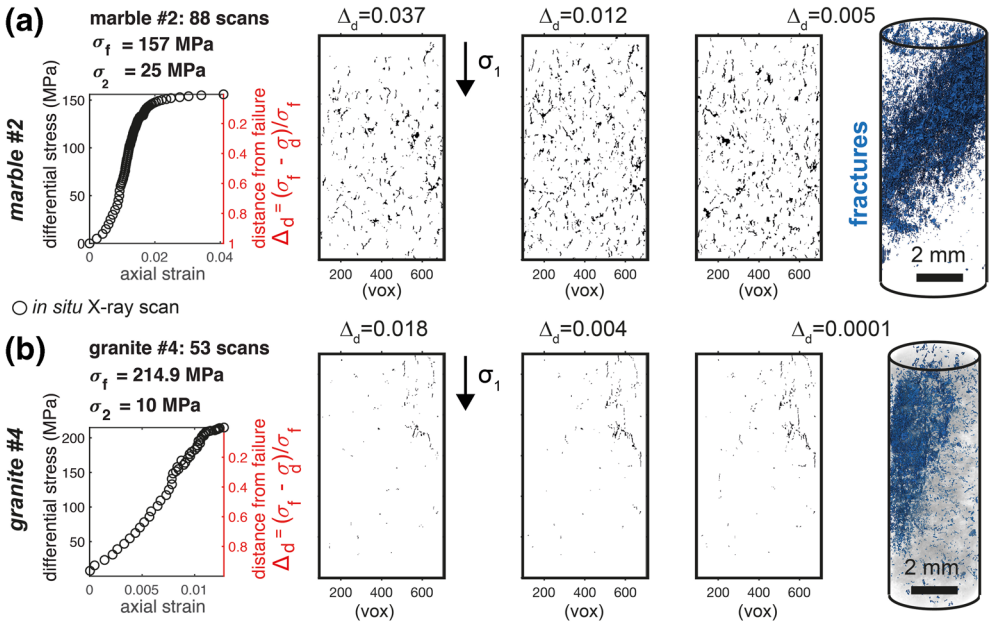

Figure 1. Mechanical history and characteristic fracture networks in experiments on marble (a) and granite (b). First column: Each black circle shows the loading conditions when an in situ X-ray tomogram was acquired. We predict the dimensionless distance from failure, Δ_d, shown in red on the right axes. 2-D slices in the second-fourth columns show the fractures and pores (black) between the solid rock (white) identified via segmentation of the tomograms. Slices are oriented parallel to the maximum compression direction (vertical), σ_1. Blue volumes in the fifth column show the location of identified fractures in the 3-D tomograms, with white or gray indicating the solid rock.

we extract a series of 41 metrics, referred to as features in the machine learning community (Tables S3 and S4). Importantly, we use failure criteria grounded in linear elastic fracture mechanics (Freund, 1998), critical phase transition (Bonamy & Bouchaud, 2011; Kandula et al., 2019; Main, 1995; Renard et al., 2018), Mohr-Coulomb (Dahlen, 1984), and strain energy density (Du & Aydin, 1993) approaches to select these metrics. We then use these features to develop XGBoost regression models (Chen & Guestrin, 2016) that predict the normalized differential stress distance to failure, $\Delta_d = \left(\sigma_f - \sigma_d\right) / \sigma_f$, where σ_f is the differential stress at macroscopic failure and σ_d is the differential stress when the tomogram was acquired. By examining the importance of the features, we identify a subset of features that have the greatest impact on predicting the proximity to failure. The relative importance of these features suggests which fracture characteristics best signal the proximity of the next macroscopic failure, and perhaps the next large earthquake. Identifying these features provides insight on the ability of existing failure criteria to predict the proximity of catastrophic failure.

2. Methods

2.1. Experimental Design

We perform eight rock deformation experiments at the X-ray tomography beamline ID19 at the European Synchrotron and Radiation Facility (ESRF). The experiments include two on Carrara marble, three on monzonite and three on Westerly granite (Table S1). Monzonite and granite have nearly identical ranges of material properties, and only differ in their mean grain size: 100–200 μm for granite and 300–400 μm for monzonite (e.g., Aben et al., 2016).

In each experiment, we impose a constant confining stress and then increase the axial stress in steps until the rock fails macroscopically. After each axial stress step, we acquire a 3-D X-ray tomogram in situ when the rock core is under load inside the deformation apparatus (Renard et al., 2016) within 2 min (Figures 1 and S1). The imposed confining stresses range from 5 to 35 MPa for each experiment (Table S2). Macroscopic

failure occurs in a sudden stress drop, typically within <0.5 MPa axial stress increase after the acquisition of the final scan.

2.2. Feature Extraction

The 3-D X-ray tomograms provide 3-D distributions of local density that we segment into voxels dominated by air (i.e., pores and fractures), and by solid (steps #1 and #2 in Figure S2). The voxel size is 6.5 μm. To assess differences in predicting failure proximity using 2-D and 3-D data, we preprocess the tomogram data into these different dimensions (Figure S2, step #3). To extract the 2-D data, we take slices parallel to the σ_1 direction (vertical) every 10 voxels, and parallel to both of the horizontal dimensions. Then we identify potential pores or fractures by finding groups of pixels with eightfold connectivity (2-D) or voxels with 26-fold connectivity (3-D). These connectivities are both the most conservative for each respective dimension, ensuring the highest level of connectivity. Next, we apply a noise threshold to remove identified connected pixels or voxels below a certain threshold. We then split the 2-D slices into subareas (squares) or 3-D volumes into subvolumes (cubes) from which we calculate statistics of the fracture characteristic populations (i.e., features). The combination of different noise thresholds and subregion sizes produce 21 different representations of each experiment (Table S3). We calculate the features using the number of voxels or pixels of each identified fracture (fracture volume or area), centroid of the fracture (clustering/localization properties), or the eigenvalues and eigenvectors of the covariance matrix of the connected voxels or pixels (orientation relative to the σ_1 direction, fracture length, fracture aperture, shape anisotropy) (Table S4). We also include a random number as feature #41 in order to compare the importance of features to a random value. Preexisting failure criteria of linear elastic fracture mechanics guided the selection of the features.

2.3. Machine Learning Model Design

We develop XGBoost regression models (Chen & Guestrin, 2016) to predict the stress distance to failure, Δ_d, from the 41 features. We predict the stress distance to failure, rather than the strain distance, because previous work found that rocks fail in a critical phase transition according to this metric (e.g., Renard et al., 2018, 2019). We perform a grid search over the hyperparameters to find the best subset of hyperparameters (Lundberg & Lee, 2017). We develop models using data from all eight experiments (Table S1). We estimate the predictive power of the features using two metrics widely used in the machine learning community: the feature importance (weight), and Shapely Additive Explanations (mean |SHAP| value) (Lundberg & Lee, 2017; Pedregosa et al., 2011). The feature importance quantifies the information gain caused by encountering the feature (Müller & Guido, 2016). Similarly, SHAP values quantify the influence of each feature on the model prediction (Lundberg & Lee, 2017).

We separate the training (80%) and testing (remaining 20%) data sets with no overlap between these two sets. Each sample provided to the models are distinct in time (stress step) and space. We split the samples randomly into training and testing data sets such that two samples that occur at the same time, but different spaces within the scan, may be separated into the different training and testing data sets. Later, we discuss the (insignificant) influence of using a different splitting technique on model performance.

3. Results

3.1. Model Success

The ability of the models to predict the proximity to failure depends on the extraction of the features from the fracture networks. To characterize the fracture network, we separate (i.e., segment) the 3-D X-ray attenuation fields of the rock samples (i.e., tomograms) into fractures or pores and solid rock (Figure 1). These tomograms provide micrometer spatial resolution 3-D images of the evolving fracture network, whereas in crustal tectonic settings we often only have 2-D observations, such as surficial fault traces or geodetic strain rates. To test the impact of this observational limitation on predicting the distance to failure, we generate 3-D and 2-D data sets from the tomograms from which we extract the fracture network characteristics. By comparing the success of models developed with the 2-D and 3-D data, we provide a quantitative comparison of using 2-D observations to predict failure of the 3-D system.

We measure the success of the models by calculating the value of the coefficient of determination, R^2, between the observed and predicted distances to failure, Δ_d. The R^2 values developed with the 2-D data ($R^2 = 0.3$–0.4) are generally lower than those of 3-D data ($R^2 = 0.4$–0.6) (Figure S3), as expected. These R^2 values indicate that the observed and predicted Δ_d have weak-moderate positive correlations to each other in the 2-D data and moderate-strong positive correlations in the 3-D data. Examination of the R^2 scores of the 3-D model predictions and observations indicate that these models produce more accurate predictions closer to failure, at lower Δ_d (Figure S4). Varying the method of splitting the data into training and testing data sets does not produce significant changes in the R^2 scores (Figure S5). For models developed with 3-D data with 3,000 voxel noise threshold and 300 voxel subvolume size, the range of the mean ± one standard deviation of the R^2 scores are 0.5–0.62 when the training and testing data sets are split randomly, and 0.35–0.6 when these data sets are split by time (Figure S5). The range in the scores are larger in the models developed with time splitting than with random splitting likely because the amount of information provided about the fracture network varies with time. As the rocks approach failure, with increasing time, more fractures develop and thus provide more samples to the machine learning models. Text S1 describes how varying the noise threshold, which determines the minimum size of fractures included in the analysis, and subregion size, which determines the volume or area over which features are extracted, influence the model success.

3.2. Predictive Power of Fracture Characteristics

To help identify the fracture network characteristics that may signal the proximity of the next catastrophic failure, and existing failure criteria that may predict this proximity, we examine the importance of the features used in the models. We identify the most predictive features for models developed with the 3-D data for the set of noise threshold and subregion size that produce the largest R^2 values. We do not focus on the 2-D models here because the largest R^2 values for these models are only near 0.4.

All of the features are calculated from statistics of fracture characteristics within a subvolume (Table S4 and Figure S2). For example, the shape anisotropies of all the fractures in a subvolume are calculated, and then the minimum, 25th percentile, 50th percentile, 75th percentile, and maximum values of the anisotropy population are reported as features in the input file fed to the models. We extract features with this method in order to constrain which statistics of a fracture network population provide the best predictive power. In addition, this approach reduces the degree to which atypical fracture characteristics influence the model success.

We estimate the predictive power of the features from the models with two metrics widely used in the machine learning community: the feature importance (weight) and Shapely Additive Explanations (mean |SHAP| value) (Lundberg & Lee, 2017; Pedregosa et al., 2011). To account for the influence of random variations that arise from splitting the data into training and testing data sets, we develop 50 unique models for the 3-D data. To compare the importance and mean |SHAP| values of features from these models, we derive a cumulative measure of importance. This cumulative R^2-weighted normalized mean |SHAP| value (or feature importance) for a feature, f, from the 50 models is $I = \sum_{m=1}^{m=50} R^2 \left(s_f \, / \, s_{\max} \right)$, where R^2 is the R^2 score, s_f is the mean |SHAP| value (or feature importance) for a given feature, s_{max} is the maximum mean |SHAP| value (or feature importance) of all the features of the model, and $m = 50$ indicates the number of models. We weight $s_f \, / \, s_{\max}$ by the R^2 of the model so that more accurate models have a greater impact on I.

Figure 2a shows the cumulative importance, I, of all of the features. We consider the features with $I > 50\%$ of the maximum value for either the mean |SHAP| value or feature importance as the most likely to successfully predict the proximity to macroscopic failure. Following this metric, the most predictive features include the minimum orientation of the minimum eigenvector of the fracture (i.e., smallest dimension of the fracture), the 75th percentile and maximum fracture aperture, the maximum shape anisotropy, and the 25th percentile of the distances between fracture centroids in a subvolume (Figure 2a). Models developed by splitting the training and testing data sets by the time to failure (Figure S5) host the same suite of most predictive features as the models shown here, which were developed by randomly splitting the data.

This identification of the most predictive features suggests that the model performance (R^2) should not decrease significantly upon removal of the remaining 37 features. We test this idea here by developing 50

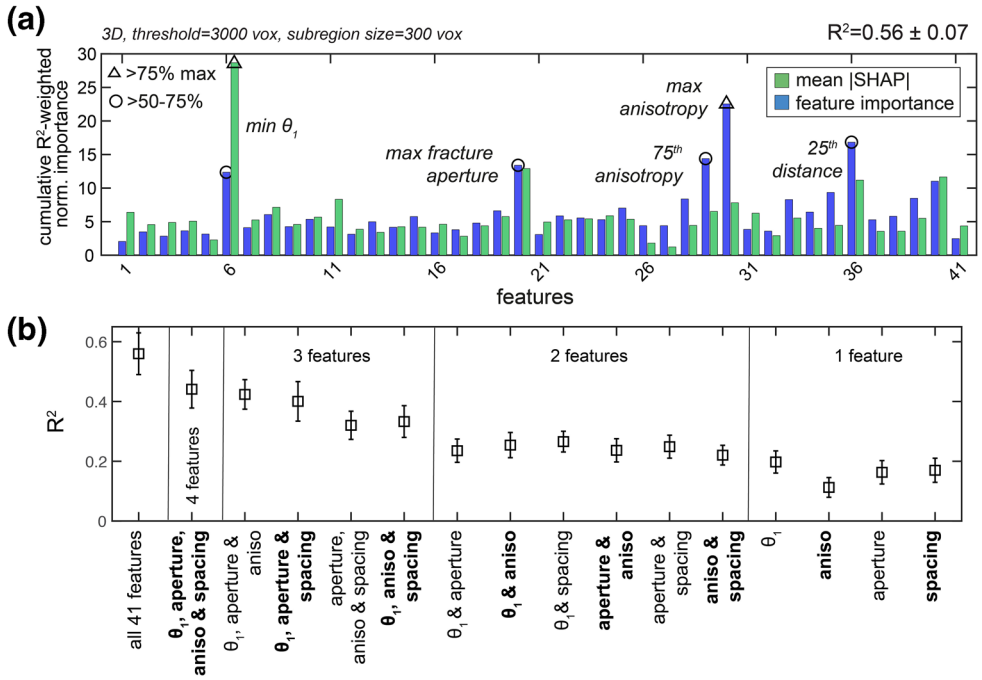

Figure 2. Influence of features on model predictions. (a) Predictive power of features in models developed from 3-D data. Green and blue bars show the cumulative R^2-weighted normalized mean |SHAP| value and feature importance, I, respectively. Triangles and circles highlight the features with $I > 75\%$ and 50–75% of the maximum values, indicating the most predictive features. Suite of I shown here is from the 3-D models with the highest R^2 scores, with the noise threshold and subvolume size shown in the upper left corner. (b) Influence of iteratively removing and combining features on the success of models. Here, θ_1, aperture, aniso., and spacing indicate the minimum θ_1, the maximum fracture aperture, maximum shape anisotropy, and 25th percentile of the distance between the fracture centroids, respectively. Black squares show the mean ± one standard deviation of R^2 for 50 models developed with each set of features.

unique models for various combinations of the four most predictive features. Removing 37 features, and including the four features identified in Figure 2a decreases the range of the mean ± one standard deviation of the R^2 of the 50 models from 0.6 to 0.5 (Figure 2b). However, developing models with only one of the four features reduces the range of R^2 to about 0.1–0.25 (Figure 2b). This trend in R^2 with various combinations of the identified most predictive features suggests that tracking only one of these features will not produce accurate estimates of the proximity to failure. Rather, successful predictions of the proximity to failure likely requires tracking all four.

3.3. Evolution of Predictive Fracture Characteristics

Following the identification of the most predictive features in the 3-D data, we now track the evolution of these fracture network characteristics throughout three example experiments on marble, monzonite, and granite. We examine the mean ± one standard deviation of the characteristics in all the subregions at each stress step (Figure S6). In 3-D, the minimum orientation of the minimum eigenvector, $\theta_1^{\min}$, evolves from generally 30° to 80° from the maximum compression direction, σ_1, near the onset of loading to 20–30° when $\Delta_d < 0.1$. When $\theta_1 = 90°$, the fracture trends vertical, with its smallest dimension (i.e., eigenvector) perpendicular to σ_1 (e.g., Figure S2). Thus, this evolution indicates that the fractures evolve from closer to vertical to more inclined relative to σ_1, and along the orientation expected to host higher magnitudes of Coulomb shear stress, when $\Delta_d < 0.1$ and thus immediately preceding macroscopic failure.

The maximum fracture aperture in a subregion accelerates from 10 to 20 voxels when $\Delta_d > 0.1$ to 20–30 voxels when $\Delta_d < 0.1$ and failure is imminent (Figure S6). This evolution indicates that fractures widen preceding macroscopic failure, and the rate of this widening increases near $\Delta_d = 0.1$. The maximum anisotropy of the fractures in a subregion also increases with loading, with a sharp increase near $\Delta_d = 0.1$. As fractures

become wider, they also lengthen, increasing their anisotropy. As fractures widen and lengthen, they also become more clustered. The fracture populations produce a clear shift in statistical properties from less clustered, with greater values of the 25th percentile of the distance between fractures in a subregion, to smaller values, again near $\Delta_d = 0.1$.

4. Discussion

4.1. Precursory Signals of the Proximity to Catastrophic Failure

The fracture network characteristics that provide the best predictive power of the stress distance to macroscopic failure include: the minimum orientation of the smallest dimension of the fracture (i.e., minimum eigenvector), the 25th percentile distance between fractures, the maximum fracture aperture, and maximum shape anisotropy of fractures in a subregion (Figure 2a). Testing the influence of removing and combining features (Figure 2b) demonstrates that predicting the stress distance to failure will be most successful with approaches that track all of these characteristics.

The observed acceleration of the maximum fracture aperture and maximum anisotropy with increasing applied differential stress (Figure S6) suggests that tracking these properties may provide robust estimates of the distance to macroscopic failure. Moreover, the evolutions of the fracture network characteristics observed in this work are similar to those observed in previous analyses (Cartwright-Taylor et al., 2020), lending confidence to the reproducibility of these trends. The fracture aperture likely correlates with the rock porosity, and thus observed geophysical precursors to some earthquakes (Aggarwal et al., 1973; Frank, 1965; Roeloffs, 1988; Whitcomb et al., 1973). The increasing anisotropy may also correlate with rock porosity because the observed concurrent increase in fracture aperture suggests that the fracture length also increases to achieve the increase in anisotropy. The spatial distribution of the fracture network also controls the magnitude of porosity. In summary, the fracture clustering, aperture, and anisotropy likely correlate with seismic velocity and porosity, and thus previously observed candidate geophysical precursors.

The tested features of the models include two classes: those that require characterizing all of the fractures in a region above some noise threshold, and those that require characterizing only the extreme values of a population. In crustal fault systems, monitoring seismic wave velocities and attenuation helps characterize the influence of all of the fractures in a crustal volume. In surface-based field analyses, characterizing only the widest or most anisotropic fractures is relatively easier than characterizing the complete network of thousands of fractures. The higher predictive power of features that involve the extreme values of a population suggests that crustal analyses that estimate the proximity of the next large earthquake may only need to focus on the extreme members of the fracture network population.

The results found here are consistent with the higher predictive power of the intermediate values of the dilatational strain identified when predicting the stress distance to failure from 3-D incremental local strain fields in 12 X-ray tomography triaxial compression experiments (McBeck et al., 2020). In those experiments, the dilatational strain provides greater predictive power than the contractive or shear strain components. This higher predictive power is consistent with the higher predictive power of fracture characteristics identified here (fracture aperture, anisotropy, clustering) that influence the porosity and elastic moduli. However, we note that some observations of crustal strain have not detected precursory deformation indicative of dilatancy (e.g., Amoruso & Crescentini, 2010), perhaps because lower strain rates suppress dilatancy (e.g., Brantut et al., 2013; Ojala et al., 2004).

The extreme values of the fracture aperture, anisotropy, and clustering provide greater predictive power than the intermediate values of these populations (Figure 2a). The widest fractures may be expected to host the most dilation, following scaling relationships between displacement and damage zone development (Savage & Brodsky, 2011). The dependence of prediction on the intermediate values of dilation (McBeck et al., 2020) suggests that the volume required to predict the distance to failure from local strain fields includes the widest fractures as well as the volume of rock surrounding them. The higher success of models developed with larger subvolume sizes presented here (Figure S3) supports the idea that characterizing deformation as strain or fractures within the volume of rock surrounding the main faults is critical to successfully predicting the proximity of the next large earthquake. Evidence from natural crustal systems supports this idea. For example, epicenters of background seismicity in the Eastern California Shear Zone

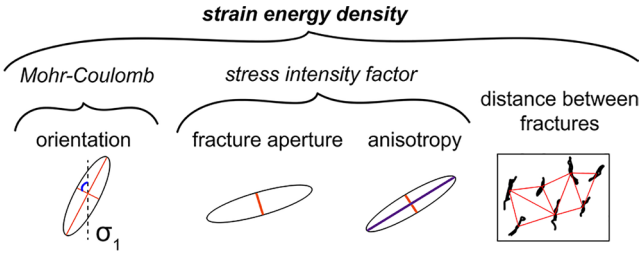

Figure 3. Recognizable predictive precursors and their relationship to existing brittle failure criteria. Strain energy density approaches tend to include the predictions of the Mohr-Coulomb criterion and the stress intensity factor, but these two approaches do not explicitly consider the spacing between fractures. The most predictive features all contribute to the strain energy density field surrounding fracture networks, and thus support using this property when predicting the stress distance to catastrophic failure.

appear to localize toward the rupture zones of large events several years before they occur (Ben-Zion & Zaliapin, 2020), highlighting the importance of analyzing deformation in crustal areas and volumes around main faults.

4.2. Assessing Failure Criteria for Predicting Failure Proximity

This machine learning analysis allows comparing the predictability of characteristics used in preexisting failure criteria of geoscience and engineering. Predictions from the Mohr-Coulomb shear failure criterion may be difficult to directly compare to those from strain energy density fields, but suites of feature importance provide direct comparisons of the fracture network characteristics that motivate these failure criteria. The highly predictive features identified here (Figure 2a) indicate that the following failure criteria provide accurate estimates of the proximity to catastrophic failure in the examined laboratory data: (1) strain energy density or stress/strain concentrations (fracture aperture, shape anisotropy, distance between fractures) (Du & Aydin, 1993; Shi, 1974), (2) stress intensity factor formulations (fracture aperture, shape anisotropy, orientation of fractures with respect to the maximum compression direction) (Freund, 1998; Isida, 1971; Raju & Newman, 1979), and (3) Mohr-Coulomb shear failure criterion (orientation of fractures) (Dahlen, 1984).

The success of the models depends on how many of the highly predictive features are included in the models (Figure 2b). In particular, the model success (R^2) using the four identified most predictive features is about five times that of the success of models developed with only one of these features. This result suggests that crustal monitoring efforts should focus on this suite of most predictive features, rather than only one of these features.

The results support predicting failure proximity using strain energy density approaches, rather than only the stress intensity factor or Mohr-Coulomb failure criterion. Strain energy density approaches will likely provide predictions that agree with the other criteria, whereas the other two methods may not identify the sites of potential failure indicated by the strain energy density (Figure 3). For example, when fractures are more anisotropic and have larger apertures, they may produce higher stress intensity factors and greater concentrations of strain energy density at their tips. When fractures are oriented closer to the optimal Coulomb orientation, they may accommodate more slip, which then also increases the strain energy density near their tips. In contrast, when two (or more) opening and slipping fractures are sufficiently close to perturb each other's stress field, they may locally develop high concentrations of strain energy density. Such fractures may not be oriented near the optimal Coulomb orientation, nor have high stress intensity factors. Thus, this work supports predicting the stress distance to failure using the strain energy density field.

The proposed success of predicting failure using the strain energy density field agrees with previous analyses that predict fault growth by identifying regions with elevated strain energy density (e.g., Du & Aydin, 1993). The integration of the strain energy density field quantifies the internal work done in the mechanical deformation of the host rock surrounding faults (Cooke & Madden, 2014). Consequently, the ability of the strain energy density field to predict the geometry of fault networks and the proximity to catastrophic failure supports the idea that energy optimization techniques can provide critical insights into rock deformation and crustal tectonic evolution (e.g., Aben et al., 2019; Del Castello & Cooke, 2007; Hardy et al., 1998; Masek & Duncan, 1998; McBeck et al., 2017, 2018; McBeck, Cordonnier, et al., 2019).

The features designed following critical phase transition approaches (total fracture volume in a subregion) (e.g., Bonamy & Bouchaud, 2011), do not have high predictive power in these models (Text S2 and Figure S7). In particular, the most predictive features of the models developed with only the marble data include the total volume of fractures in a subvolume, while the models developed with the other rocks do not. This result indicates that rocks with more homogeneous distributions of fractures may fail in a critical phase transition, whereas more heterogeneous rocks may not. The differing porosity of the rocks may also contribute to this result (e.g., Vasseur et al., 2015, 2017). Cartwright-Taylor et al. (2020) found that higher

porosity rocks fail with behavior similar to second-order or critical phase transitions, whereas lower porosity rocks and analog materials fail with behavior more similar to first-order phase transitions. The lower initial porosity of the granite and monzonite may cause these rocks to fail as first-order phase transitions, rather than critical phase transitions.

5. Conclusions

A key question is how insights into predicting the proximity of system-scale failure in laboratory experiments may be extended to predicting the proximity of crustal earthquakes. Indeed, one could divide this problem into predicting system-scale failure (the complete rock sample) and local failure (a large earthquake on one or several faults). Previous results and the work presented here support the idea that similar fracture characteristics may help predict both system-scale and local failure, at least in the laboratory. When predicting whether individual fractures will increase or decrease in volume from 3-D data in four of the experiments analyzed here, on marble, granite, and monzonite (McBeck, Kandula, et al., 2019), the identified highly predictive features are similar to those identified in the present work. The features that provide reliable estimates of whether an individual fracture grows or closes (i.e., local failure), and also the distance to failure (i.e., global failure), include the orientation, aperture, shape anisotropy, and statistics of clustering. Thus, predicting both local and global failure benefits from fracture characteristics that control the rock dilation and the strain energy density field, supporting the idea that energy optimization may help predict fault network development and the timing of large earthquakes.

Data Availability Statement

Beamtime was allocated at the European Synchrotron Radiation Facility (Long Term Proposal ES-295). The experimental data are available on Norstore (Renard, 2017, 2018)

Acknowledgments
The Norwegian Research Council (grants 272217 to F. Renard and 300435 to J. A. McBeck) and U.S. Department of Energy (award DE-SC0016520 to Y. Ben-Zion) funded this work. The authors thank reviewer Ian Main, an anonymous reviewer, and Associate Editor Germán Prieto for suggestions that improved this manuscript.

References

Aben, F. M., Brantut, N., Mitchell, T. M., & David, E. C. (2019). Rupture energetics in crustal rock from laboratory-scale seismic tomography. *Geophysical Research Letters*, *46*, 7337–7344. https://doi.org/10.1029/2019GL083040

Aben, F. M., Doan, M. L., Mitchell, T. M., Toussaint, R., Reuschlé, T., Fondriest, M., et al. (2016). Dynamic fracturing by successive coseismic loadings leads to pulverization in active fault zones. *Journal of Geophysical Research: Solid Earth*, *121*, 2338–2360. https://doi.org/10.1002/2015JB012542

Aggarwal, Y. P., Sykes, L. R., Armbruster, J., & Sbar, M. L. (1973). Premonitory changes in seismic velocities and prediction of earthquakes. *Nature*, *241*(5385), 101–104.

Amoruso, A., & Crescentini, L. (2010). Limits on earthquake nucleation and other pre-seismic phenomena from continuous strain in the near field of the 2009 L'Aquila earthquake. *Geophysical Research Letters*, *37*, L10307. https://doi.org/10.1029/2010GL043308

Ben-Zion, Y., & Zaliapin, I. (2020). Localization and coalescence of seismicity before large earthquakes. *Geophysical Journal International*, *223*(1), 561–583.

Bolt, B. A. (1977). Constancy of P travel times from Nevada explosions to Oroville dam station 1970-1976. *Bulletin of the Seismological Society of America*, *67*(1), 27–32.

Bonamy, D., & Bouchaud, E. (2011). Failure of heterogeneous materials: A dynamic phase transition? *Physics Reports*, *498*(1), 1–44.

Brantut, N., Heap, M. J., Meredith, P. G., & Baud, P. (2013). Time-dependent cracking and brittle creep in crustal rocks: A review. *Journal of Structural Geology*, *52*, 17–43.

Cartwright-Taylor, A., Main, I. G., Butler, I. B., Fusseis, F., Flynn, M., & King, A. (2020). Catastrophic failure: How and when? Insights from 4-D in situ X-ray microtomography. *Journal of Geophysical Research: Solid Earth*, *125*, e2020JB019642. https://doi.org/10.1029/2020JB019642

Chen, T., & Guestrin, C. (2016). Xgboost: A scalable tree boosting system. *In Proceedings of the 22nd ACM SIGKDD International Conference on Knowledge Discovery and Data Mining* (pp. 785–794). San Francisco, CA: ACM.

Cicerone, R. D., Ebel, J. E., & Britton, J. (2009). A systematic compilation of earthquake precursors. *Tectonophysics*, *476*(3–4), 371–396.

Cooke, M. L., & Madden, E. H. (2014). Is the Earth lazy? A review of work minimization in fault evolution. *Journal of Structural Geology*, *66*, 334–346.

Corbi, F., Sandri, L., Bedford, J., Funiciello, F., Brizzi, S., Rosenau, M., & Lallemand, S. (2019). Machine learning can predict the timing and size of analog earthquakes. *Geophysical Research Letters*, *46*, 1303–1311. https://doi.org/10.1029/2018GL081251

Dahlen, F. A. (1984). Noncohesive critical Coulomb wedges: An exact solution. *Journal of Geophysical Research*, *89*(B12), 10125–10133.

Del Castello, M., & Cooke, M. L. (2007). Underthrusting-accretion cycle: Work budget as revealed by the boundary element method. *Journal of Geophysical Research*, *112*, B12404. https://doi.org/10.1029/2007JB004997

Du, Y., & Aydin, A. (1993). The maximum distortional strain energy density criterion for shear fracture propagation with applications to the growth paths of en echelon faults. *Geophysical Research Letters*, *20*(11), 1091–1094.

Frank, F. C. (1965). On dilatancy in relation to seismic sources. *Reviews of Geophysics*, *3*(4), 485–503.

Freund, L. B. (1998). *Dynamic Fracture Mechanics* Cambridge: Cambridge University Press.

Haase, J. S., Shearer, P. M., & Aster, R. C. (1995). Constraints on temporal variations in velocity near Anza, California, from analysis of similar event pairs. *Bulletin of the Seismological Society of America*, *85*(1), 194–206.

Hardy, S., Duncan, C., Masek, J., & Brown, D. (1998). Minimum work, fault activity and the growth of critical wedges in fold and thrust belts. *Basin Research*, *10*(3), 365–373.
Hulbert, C., Rouet-Leduc, B., Johnson, P. A., Ren, C. X., Rivière, J., Bolton, D. C., & Marone, C. (2019). Similarity of fast and slow earthquakes illuminated by machine learning. *Nature Geoscience*, *12*(1), 69–74.
Isida, M. (1971). Effect of width and length on stress intensity factors of internally cracked plates under various boundary conditions. *International Journal of Fracture Mechanics*, *7*(3), 301–316.
Kandula, N., Cordonnier, B., Boller, E., Weiss, J., Dysthe, D. K., & Renard, F. (2019). Dynamics of microscale precursors during brittle compressive failure in Carrara marble. *Journal of Geophysical Research: Solid Earth*, *124*, 6121–6139. https://doi.org/10.1029/2019JB017381
Lundberg, S. M., & Lee, S. I. (2017). A unified approach to interpreting model predictions. In *Advances in Neural Information Processing Systems* (pp. 4765–4774). Long Beach, CA: Neural Information Processing Systems.
Main, I. G. (1995). Earthquakes as critical phenomena: Implications for probabilistic seismic hazard analysis. *Bulletin of the Seismological Society of America*, *85*(5), 1299–1308.
Masek, J. G., & Duncan, C. C. (1998). Minimum-work mountain building. *Journal of Geophysical Research*, *103*(B1), 907–917.
McBeck, J., Aiken, J. M., Ben-Zion, Y., & Renard, F. (2020). Predicting the proximity to macroscopic failure using local strain populations from dynamic in situ X-ray tomography triaxial compression experiments on rocks. *Earth and Planetary Science Letters*, *543*, 116344.
McBeck, J., Cooke, M., & Madden, E. (2017). Work optimization predicts the evolution of extensional step overs within anisotropic host rock: Implications for the San Pablo Bay, CA. *Tectonics*, *36*, 2630–2646. https://doi.org/10.1002/2017TC004782
McBeck, J., Cooke, M., Souloumiac, P., Maillot, B., & Mary, B. (2018). The influence of detachment strength on the evolving deformational energy budget of physical accretionary prisms. *Solid Earth*, *9*(6), 1421–1436.
McBeck, J., Cordonnier, B., Mair, K., & Renard, F. (2019). The evolving energy budget of experimental faults within continental crust: Insights from in situ dynamic X-ray microtomography. *Journal of Structural Geology*, *123*, 42–53.
McBeck, J., Kandula, N., Aiken, J. M., Cordonnier, B., & Renard, F. (2019). Isolating the factors that govern fracture development in rocks throughout dynamic in situ X-ray tomography experiments. *Geophysical Research Letters*, *46*, 11127–11135. https://doi.org/10.1029/2019GL084613
McEvilly, T. V., & Johnson, L. R. (1974). Stability of P an S velocities from Central California quarry blasts. *Bulletin of the Seismological Society of America*, *64*(2), 343–353.
Müller, A. C., & Guido, S. (2016). *Introduction to Machine Learning With Python: A Guide for Data Scientists*. Sebastopol, CA: O'Reilly Media, Inc.
Nur, A. (1974). Matsushiro, Japan, earthquake swarm: Confirmation of the dilatancy-fluid diffusion model. *Geology*, *2*(5), 217–221.
Ojala, I. O., Main, I., & Ngwenya, B. (2004). Strain rate and temperature dependence of Omori law scaling constants of AE data: Implications for earthquake foreshock-aftershock sequences. *Geophysical Research Letters*, *31*, L24617. https://doi.org/10.1029/2004GL020781
Pedregosa, F., Varoquaux, G., Gramfort, A., Michel, V., Thirion, B., Grisel, O., et al. (2011). Scikit-learn: Machine learning in Python. *Journal of Machine Learning Research*, *12*, 2825–2830.
Raju, I. S., & Newman, J. C., Jr. (1979). Stress-intensity factors for a wide range of semi-elliptical surface cracks in finite-thickness plates. *Engineering Fracture Mechanics*, *11*(4), 817–829.
Renard, F. (2017). Critical evolution of damage towards system size failure in a crystalline rock [Data set]. *Norstore*. https://doi.org/10.11582/2017.00025
Renard, F. (2018). Volumetric and shear processes in crystalline rock during the approach to faulting [Data set]. *Norstore*. https://doi.org/10.11582/2018.00023
Renard, F., Cordonnier, B., Dysthe, D. K., Boller, E., Tafforeau, P., & Rack, A. (2016). A deformation rig for synchrotron microtomography studies of geomaterials under conditions down to 10 km depth in the Earth. *Journal of Synchrotron Radiation*, *23*(4), 1030–1034.
Renard, F., McBeck, J., Kandula, N., Cordonnier, B., Meakin, P., & Ben-Zion, Y. (2019). Volumetric and shear processes in crystalline rock approaching faulting. *Proceedings of the National Academy of Sciences of the United States of America*, *116*(33), 16234–16239.
Renard, F., Weiss, J., Mathiesen, J., Ben-Zion, Y., Kandula, N., & Cordonnier, B. (2018). Critical evolution of damage toward system-size failure in crystalline rock. *Journal of Geophysical Research: Solid Earth*, *123*, 1969–1986. https://doi.org/10.1002/2017JB014964
Roeloffs, E. A. (1988). Hydrologic precursors to earthquakes: A review. *Pure and Applied Geophysics*, *126*(2–4), 177–209.
Rouet-Leduc, B., Hulbert, C., Lubbers, N., Barros, K., Humphreys, C. J., & Johnson, P. A. (2017). Machine learning predicts laboratory earthquakes. *Geophysical Research Letters*, *44*, 9276–9282. https://doi.org/10.1002/2017GL074677
Savage, H. M., & Brodsky, E. E. (2011). Collateral damage: Evolution with displacement of fracture distribution and secondary fault strands in fault damage zones. *Journal of Geophysical Research*, *116*, B03405. https://doi.org/10.1029/2010JB007665
Sih, G. C. (1974). Strain-energy-density factor applied to mixed mode crack problems. *International Journal of Fracture*, *10*(3), 305–321.
Vasseur, J., Wadsworth, F. B., Heap, M. J., Main, I. G., Lavallée, Y., & Dingwell, D. B. (2017). Does an inter-flaw length control the accuracy of rupture forecasting in geological materials? *Earth and Planetary Science Letters*, *475*, 181–189.
Vasseur, J., Wadsworth, F. B., Lavallée, Y., Bell, A. F., Main, I. G., & Dingwell, D. B. (2015). Heterogeneity: The key to failure forecasting. *Scientific Reports*, *5*(1), 1–7.
Whitcomb, J. H., Garmany, J. D., & Anderson, D. L. (1973). Earthquake prediction: Variation of seismic velocities before the San Francisco earthquake. *Science*, *180*(4086), 632–635.